Systems & Control Transactions

Research Article - Peer Reviewed Conference Proceeding
ESCAPE 35 - European Symposium on Computer Aided Process Engineering
Ghent, Belgium. 6-9 July 2025
Jan F.M. Van Impe, Grégoire Léonard, Satyajeet S. Bhonsale,
Monika E. Polańska, Filip Logist (Eds.)

PSE PRESS

Enhanced Computational Approach for Simulation and Optimisation of Vacuum (Pressure) Swing Adsorption

Yangyanbing Liao, Andrew Wright, and Jie Li*

The University of Manchester, Centre for Process Integration, Department of Chemical Engineering, Manchester, UK
* Corresponding Author: jie.li-2@manchester.ac.uk.

ABSTRACT

Vacuum (pressure) swing adsorption (V(P)SA) has received considerable attention in the past decades. Existing studies typically estimate vacuum pump energy consumption using an approximate constant energy efficiency or an empirical energy efficiency correlation, leading to inaccurate representation of realistic vacuum pump performance. In this paper an enhanced computational approach is proposed for simulation and optimisation of V(P)SA through simultaneous integration of realistic vacuum pump data and adsorption bed fluidisation limits. The computational results show that the developed prediction models accurately represent the actual performance curves of the vacuum pump. Incorporation of the vacuum pump prediction models and fluidisation constraints in V(P)SA optimisation leads to significantly different optimal solutions compared to when these factors are not considered.

Keywords: Pressure swing adsorption, Process simulation, Optimization, Vacuum pump modelling, bed fluidization

INTRODUCTION

Vacuum (pressure) swing adsorption (V(P)SA) has received considerable attention for gas separation and purification in the past decades [1]. Mathematical modelling of V(P)SA involves description of the spatial and temporal evolution of mass, momentum and energy, resulting in coupled stiff hyperbolic/parabolic partial differential equations (PDEs). Auxiliary nonlinear equations including gas adsorption isotherms and pressure drop correlations are also included to complement process dynamics [2].

In most existing V(P)SA models, a time-dependent pressure profile or a fixed flow rate is used in the boundary conditions (BCs) at the vacuum pump end of the adsorption bed to estimate the performance of a real vacuum pump. With these predefined BCs, the total energy consumption of the vacuum pump is then determined by dividing the isentropic gas compression work by an estimated energy efficiency. It is reported that the vacuum pump can contribute at least 60% to the overall energy consumption in a VSA cycle for CO_2 capture [3]. Hence, accurate estimation of the vacuum pump efficiency and quantification of its energy consumption are crucial for the economic analysis of the V(P)SA processes.

Most existing computational studies on V(P)SA have assumed constant vacuum pump efficiency ranging from 60% to 100% where the vacuum pump efficiency of 72% was most used [4]. However, 72% is a typical efficiency value for compressors, instead of vacuum pumps [5]. A low efficiency of 30% was reported [5]. All these have indicated that the energy consumption of the vacuum pump could have been underestimated by at least a factor of two in many existing computational studies.

Instead of assuming a constant vacuum pump efficiency, an efficiency correlation has been developed to more accurately evaluate the vacuum pump performance. It has been observed that the efficiency tends to remain constant around 80% when the inlet pressure of the vacuum pump approaches 1 atm, whilst decreasing sharply to a very low value (e.g., below 20%) at lower pressures [6]. An empirical correlation was thus derived to relate the vacuum pump efficiency to the inlet pressure. However, their correlation fails to conform to the trend suggested by the data points at higher pressures due to significant deviations between data points and model predictions at high pressures.

The adsorption bed fluidisation is another key factor that must be accounted for in designing and operating

the V(P)SA process. This is because bed fluidisation incurs rapid adsorbent attrition and eventually results in a substantial decrease in the separation performance [7]. Nevertheless, only a few have considered the impact of bed fluidisation. They considered the effects of bed fluidisation at specific stages in PSA simulation. However, bed fluidisation can occur at any point along the bed during any step [8]. In other words, fluidisation may be experienced at certain points along the bed during certain steps in the above studies.

To address the above research gaps, in this work we first employ the data-driven modelling approach [9,10] to develop prediction models for the pumping speed and power of the vacuum pump based on real performance curves. This approach enables accurate predictions of the vacuum pump's flow rate and energy consumption. We then develop a new, comprehensive V(P)SA mathematical formulation with incorporation of the proposed vacuum pump performance models. This allows for an accurate evaluation of the V(P)SA process performance without relying on estimated vacuum pump energy efficiency or pressure/flow rate BCs at the vacuum pump end of the adsorption bed. To determine the optimal operating conditions and prevent bed fluidisation, we then construct a new optimisation problem that simultaneously incorporates the proposed V(P)SA model and the bed fluidisation constraints. To the best of our knowledge, this is the first work that considers simultaneously real vacuum pump performance data and bed fluidisation in V(P)SA optimisation. The capability of the developed V(P)SA model is illustrated through a case study.

PROBLEM STATEMENT

A PSA process operates cyclically with three fundamental steps, including pressurisation, high-pressure adsorption, low-pressure regeneration. Some complementary steps such as pressure equalisation, rinse and purge are included to enhance process performance. An example of the 4-step PSA cycle is illustrated in Figure 1. This cycle involves adsorption, blowdown, evacuation and feed pressurisation. The problem can be stated below:

Given:

1. The number of adsorption bed, and bed configuration.
2. Feed conditions such as flow rate, composition, temperature, and pressure.
3. Adsorbent layers, physical properties of the adsorbent and the corresponding adsorption isotherms.
4. Product purity and recovery requirements.

Determine:

1. The time for each step.
2. Operating conditions, such as operating pressures and feed flow velocity.

For the illustrative example of the 4-step PSA cycle, the decision variables would be the time required for pressurisation, high-pressure adsorption, blowdown, and evaluation, the high adsorption pressure, the intermediate pressure, and the low pressure and the interstitial feed velocity. The degree of freedom is 8.

Assumptions:

- Gas phase follows ideal gas law.
- Non-isothermal adsorption process.
- The bulk flow pattern follows a plug flow model.
- The adsorption equilibrium is described by a dual-site Langmuir model with pure component isotherms dependent on gas phase concentration.
- The mass transfer is described by a linear driving force (LDF) model where the mass transfer resistance is controlled by the molecular diffusion in the macropores.
- The heat of adsorption of each gas component is constant.
- Instantaneous heat transfer between bulk fluid and adsorbent.
- Uniform bed with constant bed void fraction, particle porosity and particle size.
- No radial gradients in concentration, temperature, or pressure.

The objective is to minimise the energy penalty or cost. Other objectives such as minimize total annualised cost can also be employed.

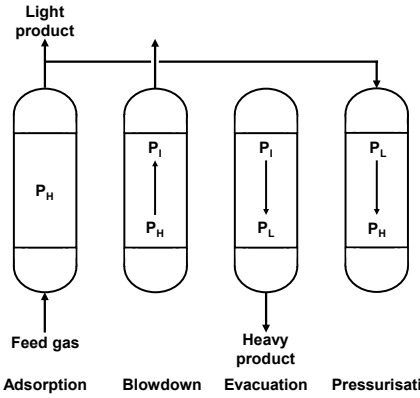

Figure 1. Example of a 4-step V(P)SA cycle.

MATHEMATICAL FORMULATION FOR V(P)SA SIMULATION AND OPTIMISATION

Rigorous PSA model

The dimensionless model equations for a general PSA process are provided as follows,

$$\frac{\partial y_i}{\partial \tau} = -\frac{\bar{T}}{\bar{P}}\frac{\partial}{\partial Z}\left(\frac{y_i \bar{P}}{\bar{T}}\bar{v}\right) - \psi\frac{\bar{T}}{\bar{P}}\frac{\partial x_i}{\partial \tau} - \frac{y_i}{\bar{P}}\frac{\partial \bar{P}}{\partial \tau} + \frac{y_i}{\bar{T}}\frac{\partial \bar{T}}{\partial \tau} \quad (1)$$

$$\frac{\partial \bar{P}}{\partial \tau} = -\bar{T}\frac{\partial}{\partial Z}\left(\frac{\bar{P}}{\bar{T}}\bar{v}\right) - \psi\bar{T}\sum_i^{n_{comp}}\frac{\partial x_i}{\partial \tau} + \frac{\bar{P}}{\bar{T}}\frac{\partial \bar{T}}{\partial \tau} \quad (2)$$

$$\frac{\partial \bar{T}}{\partial \tau} = -\Omega_1\frac{\partial}{\partial Z}(\bar{v}\bar{P}) - \Omega_2\bar{T}\sum_i^{n_{comp}}\frac{\partial x_i}{\partial \tau} + \sum_i^{n_{comp}}\left(\sigma_i\frac{\partial x_i}{\partial \tau}\right) - \Omega_3(\bar{T} - \bar{T}_w) - \Omega_1\frac{\partial \bar{P}}{\partial \tau} \quad (3)$$

$$\frac{\partial x_i}{\partial \tau} = \alpha_i(x_i^* - x_i) \quad (4)$$

$$q_i^* = \frac{q_{sb,i}b_i c_i}{1+\sum_{i=1}^{n_{comp}} b_i c_i} + \frac{q_{sd,i}d_i c_i}{1+\sum_{i=1}^{n_{comp}} d_i c_i} \quad (5)$$

$$-\frac{\partial \bar{P}}{\partial Z} = \frac{150}{4}\frac{1}{r_p^2}\left(\frac{1-\varepsilon}{\varepsilon}\right)^2\frac{v_0 z_0}{P_0}\mu\bar{v} + \frac{1.75}{2}\frac{1}{r_p}\left(\frac{1-\varepsilon}{\varepsilon}\right)\rho_g|\bar{v}|\bar{v} \quad (6)$$

Equation (1) is mass balance for each component. (2) is momentum balance equation. (3) is bed energy balance equation. (4) is linear driving force. (5) is adsorption isotherm equation. (6) is the Ergun equation for pressure drop. The boundary conditions for each cycle will be referred to [4].

We assume that the adsorption bed is connected directly to the vacuum pump with no pressure drop between them (see Figure 2). Given the same temperature, the outlet volumetric flow rate and pressure of the adsorption bed are equal to the inlet volumetric flow rate and pressure of the vacuum pump, respectively, as specified by Eqs. (7) and (8). In Figure 4, $Z = 0$ represents the vacuum pump end of the adsorption bed, $P_{out,B}$ and $V_{out,B}$ are the outlet pressure and volumetric flow rate of the bed, $P_{in,VP}$ and $V_{in,VP}$ are the inlet pressure and volumetric flow rate of the vacuum pump, and P_{dis} is the discharge pressure of the vacuum pump, which is assumed to be equal to the atmospheric pressure, $P_{atm} = 1$ bar.

$$P_{out,B} = P_{in,VP} \quad (7)$$

$$V_{out,B} = V_{in,VP} \quad (8)$$

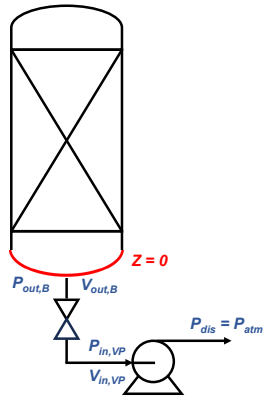

Figure 2. Direct connection between the adsorption bed and a vacuum pump

The inlet volumetric flow rate of the vacuum pump ($V_{in,VP}$) must satisfy the vacuum pump pumping speed prediction model, as shown by Eq. (10), where $f_1(P_{in,VP})$ represents the best model developed.

$$V_{in,VP} = f_1(P_{in,VP}) \quad (9)$$

At the vacuum pump end, the outlet flow rate of the bed needs to satisfy the pressure drop correlation $f_2(P_{out,B})$, as shown by Eq. (9), which is usually the Ergun equation [Eq. (6)] or Darcy's law.

$$V_{out,B} = f_2(P_{out,B}) \quad (10)$$

$V_{out,B}$ and $P_{in,VP}$ can be computed by combining Eqs. (7)-(10). It should be noted that the pumping speed curves are normally measured at 298.15 K and 1 atm. Therefore, the volumetric flow rate must be converted to match the corresponding operating conditions.

Given $V_{out,B}$, the outlet interstitial velocity of the adsorption bed $V_{out,B}$ can be computed:

$$v_{out,\,B} = \frac{V_{out,B}}{\varepsilon A} \quad (11)$$

where ε is the adsorption bed void fraction, and A is the cross-section area of the column.

We define $PW_{tot,VP}$ as the total power required by the vacuum pump, which can be evaluated by the power prediction model, $f_3(P_{in,VP})$, as shown by Eq. (12).

$$PW_{tot,VP} = f_3(P_{in,VP}) \quad (12)$$

The instantaneous isentropic gas compression power ($PW_{isen,VP}$) can be evaluated using Eq. (13).

$$PW_{isen,VP} = \frac{\kappa}{\kappa-1}P_{in,VP}\cdot\varepsilon\cdot\pi\cdot r_{in}^2\cdot v_{out,B}\left[\left(\frac{P_{dis}}{P_{in,VP}}\right)^{\frac{\kappa-1}{\kappa}} - 1\right] \quad (13)$$

where κ represents the gas isentropic constant, and r_{in} is the inner radius of the column.

The instantaneous vacuum pump efficiency, η_{VP}, is therefore defined as the ratio of the isentropic gas compression power to the total vacuum pump power.

$$\eta_{VP}(\%) = \frac{PW_{isen,VP}}{PW_{tot,VP}} \times 100\% \quad (14)$$

Based on the instantaneous values from Eqs. (13) and (14), Eqs. (15) and (16) are used to compute the total energy consumption and the time-averaged efficiency of the vacuum pump:

$$E_{tot,VP} = \int_{t_{ini}}^{t_f} PW_{tot,VP}\,dt \quad (15)$$

$$\eta_{ave,VP}(\%) = \frac{1}{t_f - t_{ini}}\int_{t_{ini}}^{t_f}\eta_{VP}\,dt \quad (16)$$

where t_{ini} and t_f represent the initial and final time points between which the vacuum pump operates, $E_{tot,VP}$ is the total vacuum pump energy consumption, and $\eta_{ave,VP}$ is

the time-averaged efficiency of the vacuum pump over the period between t_{ini} and t_f, respectively.

Adsorption Bed Fluidisation

The adsorption bed fluidisation is characterised by the approach to fluidisation (ATF):

$$ATF = \frac{\frac{\partial P}{\partial Z}\big|_{local}}{\frac{\partial P}{\partial Z}\big|_{min.fluid}} \tag{17}$$

where $\frac{\partial P}{\partial Z}\big|_{local}$ denotes the pressure gradient at a specific location in the bed, and $\frac{\partial P}{\partial Z}\big|_{min.fluid}$ is the minimum fluidisation pressure gradient in the upflow direction.

$$-\frac{\partial P}{\partial Z}\big|_{min.fluid} = (\rho_g - \rho_s) \cdot (1-\varepsilon) \cdot g \tag{18}$$

where ρ_g and $\rho_s$are the density of gas and adsorbent, respectively; ε is the bed void fraction; g is the gravitational constant. Eq. (18) essentially states that bed fluidisation occurs when the upward force exerted on a section of the bed offsets its gravity due to the pressure drop.

To prevent the onset of fluidisation, the ATF value should be limited within some values in the upflow and downflow operations, respectively.

$$ATF_{up} \leq \theta_{up} \tag{19}$$

$$ATF_{down} \leq \theta_{down} \tag{20}$$

where ATF_{up} and ATF_{down} represent the ATF value in the upflow and downflow directions, respectively.

Additional constraints

The following constraints are imposed in addition to the V(P)SA model. First, the required product purity and recovery must be satisfied.

$$Purity \geq Purity_{req}^{tar} \tag{21}$$

$$Recovery \geq Recovery_{req}^{tar} \tag{22}$$

$$\begin{aligned} Purity &= \frac{Moles\ of\ target\ gas\ in\ product}{Total\ moles\ of\ product} \\ &= \frac{\frac{\varepsilon A}{R}\int_0^{t_p} \frac{v_{out} \cdot y_{out,i} \cdot P_{out}}{T_{out}} dt}{\frac{\varepsilon A}{R}\int_0^{t_p} \frac{v_{out} \cdot P_{out}}{T_{out}} dt} \end{aligned} \tag{23}$$

$$\begin{aligned} &Recovery \\ &= \frac{Moles\ of\ target\ gas\ in\ product}{Total\ moles\ of\ target\ gas\ fed} \\ &= \frac{\frac{\varepsilon A}{R}\int_0^{t_p} \frac{v_{out} \cdot y_i \cdot P_{out}}{T_{out}} dt}{\frac{\varepsilon A}{R}\sum_{j=1}^{n_{step}} \int_0^{t_f} \frac{v_f^j \cdot y_{f,i}^j \cdot P_f^j}{T_f^j} dt} \end{aligned} \tag{24}$$

where $Purity^{tar}$ and $Recovery^{tar}$ are are the purity and recovery of the target gas, and $Purity_{req}^{tar}$ and $Recovery_{req}^{tar}$ denote the required purity and recovery.

We also constrain the bed length-to-diameter ratio (L/D) to either a fixed value or within specified bounds.

The lower and upper bounds are imposed for all decision variables, generally represented by a vector $\mathbf{x}$.

$$\mathbf{x}^{lb} \leq \mathbf{x} \leq \mathbf{x}^{ub} \tag{25}$$

where $\mathbf{x}$ is a vector of all decision variables, $\mathbf{x}^{lb}$ and $\mathbf{x}^{ub}$ are the lower and upper bounds. The V(P)SA optimisation problem (denoted as **P**) is defined as follows:

$$\begin{aligned} min \quad & obj \\ s.t. \quad & \text{PSA model equations } 1-6 \\ & \text{Eqs. } 7-11, \text{or estimated vacuum pump efficiency} \\ & \text{Equations } 12-24 \\ & L/D = R_{fixed} \text{ or } R^{lb} \leq L/D \leq R^{ub} \\ & \text{Boundary conditions in [4]} \\ & \mathbf{x}^{lb} \leq \mathbf{x} \leq \mathbf{x}^{ub} \end{aligned}$$

where obj is the objective function, which usually denotes the total cost. Genetic algorithm (GA) in MATLAB is used to solve the optimisation problem **P** with a population size of 24 times of the number of decision variables and a maximum generation of 50 [3].

It should be noted that the V(P)SA model **P** enables computation of the instantaneous outlet gas velocity and pressure of the adsorption bed on the vacuum pump end. As a result, an estimated boundary condition, such as a constant flow rate or a predefined pressure profile, is not required. It enables accurate evaluation of the vacuum pump pumping speed and energy consumption, from which the vacuum pump efficiency is determined post-simulation. This contrasts with the common approaches where predefined estimations of the necessary BCs and vacuum pump efficiency are required in previous studies.

RESULTS AND DISCUSSION

Performance Prediction Models of Vacuum Pumps

After reviewing a large number of vacuum pump vendor manuals, ten vacuum pump performance curves are identified, which account for a broad range of the pumping speed. The ten vacuum pumps are given below,

- Leybold DRYVAC DV 800 screw vacuum pump
- Leybold LEYVAC LV 140 screw vacuum pump (50 Hz)
- Leybold LEYVAC LV 140 screw vacuum pump (60 Hz)
- Zhaohan 2BE1 202 liquid ring pump (790 RPM)
- Zhaohan 2BE1 202 liquid ring pump (880 RPM)
- Edwards EDS 300 dry screw vacuum pump
- Edwards EDS 480 dry screw vacuum pump

- Edwards nXDS20i dry scroll vacuum pump
- Edwards nXDS15i dry scroll vacuum pump
- Edwards nXDS10i dry scroll vacuum pump

Data points are extracted from each performance curve using WebPlotDigitizer to establish the prediction models of vacuum pump pumping speed and power (i.e., eqs. 10 and 12) using the data-driven approach [9,10]. The training and test results for pumping speed are provided in Table 1. It is quantitatively shown that each performance model demonstrates close agreement with the data, as indicated by the low RMSE values and coefficient of determination (R^2) values near 1.

Table 1. Training and test results

Pump	Pumping speed			
	Training		Test	
	R^2	RMSE	R^2	RMSE
DV 800	0.9998	3.18	0.9985	9.0900
50 Hz	1.0000	0.14	0.9998	0.4866
60Hz	1.0000	0.09	1.0000	0.2588
790 RPM	0.9997	4.1074	0.9965	4.1737
880 RPM	0.9992	1.5844	0.9992	1.7538
EDS 300	0.9999	0.5709	0.9996	1.5020
EDS 480	0.9999	1.0752	0.9995	2.7210
nXDS20i	0.9998	0.0774	0.9995	0.1294
nXDS15i	0.9999	0.0414	0.9998	0.0658
nXDS10i	0.9999	0.0348	0.9997	0.0550

VPSA Optimization Results

We take the VSA cycle from [3] to illustrate the process optimisation results by simultaneously considering the vacuum pump performance prediction models and the fluidisation constraints. The VSA cycle is illustrated in Figure 1. The feed gas mixture, consisting of 20% CO_2 and 80% N_2, enters the bed at 313.15 K. Parameters such as the adsorbent physical properties, adsorption isotherms, column configuration are adapted from [3]. The objective function is CO_2 capture cost from [3].

We compare the optimisation results by using a constant efficiency of 72%, the efficiency correlation from [6], and the developed V(P)SA model involving vacuum pump performance models, respectively. The constant efficiency of 72% is used in case 1, whilst the correlation from [6] is used in case 2. The developed V(P)SA model is used in case 3. The objective is to minimise the CO_2 capture cost [3]. The purity and recovery of product CO_2 are required to be at least 0.95 and 0.90, respectively. The length-to-diameter ratio is fixed at 3 [3].

Table 2. Optimisation results for cases 1-4 with fluidisation constraints

Case	1	2	3	4
Vacuum pump efficiency	72%	–	–	36%
Operating conditions				
Fixed variables				
Length-to-diameter ratio (–)	3	3	3	3
Decision variables				
Adsorption time (s)	351	349	357	364
Pressurisation time (s)	58	54	58	64
Blowdown outlet velocity (m s^{-1})	0.94	0.94	–	0.77
Evacuation outlet velocity (m s^{-1})	1.49	1.40	–	1.23
Intermediate pressure (bar)	0.05	0.06	0.11	0.07
Low pressure (bar)	0.02	0.02	0.03	0.02
Feed velocity (m s^{-1})	0.48	0.50	0.50	0.50
Column length (m)	6.73	6.01	3.97	5.51
Dependent variables				
Maximum feed pressure (bar)	1.16	1.15	1.11	1.17
Blowdown time (s)	225	188	212	190
Evacuation time (s)	560	588	1406	665
Blowdown outlet velocity (m s^{-1})	–	–	0.39	–
Evacuation outlet velocity (m s^{-1})	–	–	0.41	–
Train configuration				
No. of columns per train (–)	4	4	6	4
No. of parallel trains (–)	188	231	543	274
Total adsorbent volume (m^3)	12602	11028	11208	10080
Process performance				
Purity (%)	95.01	95.03	95.01	95.01
Recovery (%)	90.08	90.02	90.04	90.01
Productivity (mol m^{-3} s^{-1})	0.09	0.11	0.11	0.12
Overall power consumption (MW_e)	36.43	57.56	43.84	58.67
Overall time-averaged efficiency (%)	–	42.12	36.14	–
Approach to fluidisation (ATF)				
Upflow				
Maximum adsorption ATF	0.35	0.44	0.60	0.56
Maximum blowdown ATF	0.73	0.74	0.35	0.55
Downflow				
Maximum evacuation ATF	0.86	0.80	0.20	0.69
Maximum pressurisation ATF	1.48	1.51	1.31	1.35
CO_2 capture cost (€/$t_{CO2,\ avoided}$)	60.93	69.56	131.23	74.86

The optimisation results for cases 1-3 are provided in Table 2. When the constant efficiency of 72% and the efficiency correlation from [6] are used (i.e., cases 1-2),

the resulting vacuum pressure P_L is 0.02 bar and the evacuation time is significantly longer than the blowdown time. These results correspond to the fact that deep vacuum and long evacuation are necessary to satisfy purity and recovery requirements. the lowest CO_2 capture cost of 60.93 €/tCO_2, avoided is achieved in case 1 with the constant efficiency of 72%. The cost in case 2 is 69.56 €/tCO_2, avoided, which is 14% higher than that in case 1. The CO_2 capture cost in case 3 is 131.23 €/tCO_2, avoided, which is the highest cost among these three cases. This is primarily due to the low outlet interstitial velocity in the blowdown and evacuation steps when using the DV 800 vacuum pump. The low flow rate eventually leads to longer blowdown and evacuation, which greatly increases the number of columns required to process the same amount of feed gas, resulting in a higher column cost and fixed operating cost.

We use the time-averaged efficiency of 36% obtained from case 3 as a constant efficiency to further illustrate the importance and effectiveness of incorporating the proposed vacuum pump performance models. The illustration is created as case 4. The optimisation results for case 4 are also provided in Table 2. The CO_2 capture cost is 74.86 €/tCO_2, avoided in case 4, which is 43% lower than 131.23 €/tCO_2, avoided in case 3. This indicates that the CO_2 capture cost can be significantly underestimated even when a well-estimated efficiency value is used. From Table 2, it is shown that the maximal ATF values in all cases have been constrained within the critical thresholds (i.e., 0.8 in the upflow and 1.8 in the downflow) at the final optimal solutions. The maximal ATF values in the pressurisation step remain the highest, as a sufficiently low P_L is essential for satisfying both purity and recovery requirements.

We also compare the optimisation results without consideration of adsorption bed fluidisation, which are presented in Table 3. By comparing results in Tables 2 and 3, the duration of each step has been significantly extended to achieve lower ATF values. Notably, the adsorption time is 350, 348, 356 and 364 s for cases 1-4, respectively, which has been increased by 130% for case 3, and at least 160% for cases 1-2 and 4. The pressurisation time, which is an additional decision variable, increases less significantly from a fixed value of 30 s in Table 3 to ~60 s in Table 2, due to a slightly larger difference between P_I and P_L. To maintain a small pressure drop across the bed and reduce the fluidisation level during the adsorption step, the feed velocity in Table 2 becomes almost half of that in Table 3 (i.e., 0.48 vs. 1.08 m s^{-1} for case 1, 0.50 vs. 1.04 m s^{-1} for case 2, 0.50 vs. 1.05 m s^{-1} for case 3 and 0.50 vs. 0.99 m s^{-1} for case 4), which in turn increases the number of parallel trains and the amount of the adsorbent required, leading to higher column and adsorbent costs. As a result, the optimal CO2 capture costs for cases 1-4 are increased by at least 16% compared those in Table 3. These results show that incorporating fluidisation constraints into PSA optimisation leads to substantial differences in the optimal solution, indicating a significant impact on PSA design.

Table 3. Optimisation results for cases 1-4 without fluidisation constraints

Case	**1**	**2**	**3**	**4**
Vacuum pump efficiency	72%	–	–	36%
Operating conditions				
Fixed variables				
Length-to-diameter ratio (–)	3	3	3	3
Decision variables				
Adsorption time (s)	127	133	156	134
Blowdown outlet velocity (m s^{-1})	1.71	1.47	–	1.49
Evacuation outlet velocity (m s^{-1})	1.29	1.20	–	0.77
Intermediate pressure (bar)	0.05	0.05	0.12	0.05
Low pressure (bar)	0.03	0.03	0.03	0.04
Feed velocity (m s^{-1})	1.08	1.04	1.05	0.99
Column length (m)	5.84	5.81	3.73	5.55
Dependent variables				
Maximum feed pressure (bar)	1.46	1.43	1.27	1.36
Blowdown time (s)	119	130	167	126
Evacuation time (s)	486	512	1237	653
Blowdown outlet velocity (m s^{-1})	–	–	0.44	–
Evacuation outlet velocity (m s^{-1})	–	–	0.47	–
Train configuration				
Number of columns per train (–)	7	7	11	8
Number of parallel trains (–)	94	101	259	119
Total adsorbent volume (m^3)	6368	7605	8116	8947
Process performance				
Purity (%)	95.02	95.00	95.00	95.00
Recovery (%)	90.01	90.00	90.00	90.01
Productivity (mol m^{-3} s^{-1})	0.16	0.15	0.15	0.13
Overall power consumption (MW_e)	30.75	43.68	44.52	51.62
Overall time-averaged efficiency (%)	–	44.67	36.22	–
Approach to fluidisation (ATF)				
Upflow				
Maximum adsorption ATF	1.21	1.12	1.35	1.00
Maximum blowdown ATF	1.66	1.34	1.09	1.44
Downflow				
Maximum evacuation ATF	0.58	0.54	0.23	0.41
Maximum pressurisation ATF	2.29	2.29	2.08	2.29
VSA capture cost (€/$t_{CO2,\ avoided}$)	46.53	52.69	113.97	65.25

CONCLUSION

In this work, we developed an enhanced computational approach for simulation and optimisation of the vacuum (pressure) swing adsorption (V(P)SA) by incorporating both the realistic vacuum pump performance prediction models and adsorption bed fluidisation constraints. The computational results demonstrated that the predictions from the developed performance prediction models closely matched the vacuum pump data. The

developed V(P)SA model did not assume an estimated energy efficiency or predefined pressure/flow rate boundary conditions for the vacuum pump. The vacuum pump efficiency typically falls in the range of 20% to 40%. This is consistent with the efficiency of 30% reported in a pilot study. When an estimated vacuum pump efficiency was applied, the optimal CO_2 capture cost was underestimated by at least 42%. It was found that bed fluidisation occurs when using a large rate of change in the pressure boundary conditions, or a vacuum pump with an excessively high pumping speed. Incorporating the vacuum pump performance prediction models and accounting for bed fluidisation constraints have a significant impact on V(P)SA optimisation outcomes, with the optimal solution varying considerably under different conditions. Future research will integrate vacuum pump performance prediction models into industrial-scale V(P)SA simulations to further evaluate the effectiveness of the proposed computational approach.

ACKNOWLEDGEMENTS

Jie Li would like to appreciate the financial support from UKRI Impact Acceleration Account (IAA 424).

REFERENCES

1. Beck J, Friedrich D, Brandani S, Guillas S, Fraga ES. Surrogate based optimisation for design of pressure swing adsorption systems. Comput. Aided Chem. Eng. xx:1217-1221 (2012) https://doi.org/10.1234/56789.10
2. Ruthven DM. PRINCIPLES OF ADSORPTION AND ADSORPTION PROCESSES. John Wiley & Sons (1984).
3. Subraveti SG, Roussanaly S, Anantharaman R, Riboldi L, Rajendran A. Techno-economic assessment of optimised vacuum swing adsorption for post-combustion CO2 capture from steam-methane reformer flue gas. Separation and Purification Technology **256**:117832 (2021).
4. Haghpanah R, Majumder A, Nilam R, et al. Multiobjective optimization of a four-step adsorption process for postcombustion CO2 capture via finite volume simulation. Ind. Eng. Chem. Res. **52**(11):4249-65 (2013).
5. Krishnamurthy S, Rao VR, Guntuka S, et al. CO2 capture from dry flue gas by vacuum swing adsorption: a pilot plant study. AIChE Journal **60**(5):1830-42 (2014).
6. Maruyama RT, Pai KN, Subraveti SG, Rajendran A. Improving the performance of vacuum swing adsorption based CO2 capture under reduced recovery requirements. International Journal of Greenhouse Gas Control **93**:102902 (2020).
7. Liu Y, Zheng X, Dai R. Numerical study of flow maldistribution and depressurization strategies in a small-scale axial adsorber. Adsorption **20**:757-68 (2014).
8. Marcinek A, Bárcia P, Guderian J. Scale-up analysis of a twin-bed PSA pilot plant. Adsorption **29**(3):125-39 (2023).
9. Li J, Xiao X, Boukouvala F, et al. Data - driven mathematical modeling and global optimization framework for entire petrochemical planning operations. AIChE Journal **62**(9):3020-40 (2016).
10. Wang W, Ma Y, Maroufmashat A, Zhang N, Li J, Xiao X. Optimal design of large-scale solar-aided hydrogen production process via machine learning based optimisation framework. Applied Energy **305**:117751 (2022).

© 2025 by the authors. Licensed to PSEcommunity.org and PSE Press. This is an open access article under the creative commons CC-BY-SA licensing terms. Credit must be given to creator and adaptations must be shared under the same terms. See https://creativecommons.org/licenses/by-sa/4.0/